Simulation of the Indian Monsoon and its Variability during the last Millennium

S. Polanski[1], B. Fallah[1], S. Prasad[2], and U. Cubasch[1]

[1]{Institute of Meteorology, Freie Universität Berlin, Germany}

[2]{German Research Center for Geosciences (GFZ), Potsdam, Germany}

Correspondence to: S. Polanski (stefan.polanski@met.fu-berlin.de)

Abstract

The general circulation model ECHAM5 has been used to simulate the Indian monsoon and its variability during the Medieval Warm Period (MWP; 900-1100 AD), the Little Ice Age (LIA; 1515-1715 AD) and for recent climate (REC; 1800-2000 AD). The focus is on the analysis of external drivers and internal feedbacks leading to extreme rainfall events over India from interannual to centennial time scale. An evaluation of spatiotemporal monsoon patterns with present-day observation data is in agreement with other state-of-the-art monsoon modeling studies. The simulated monsoon intensity on centennial time scale is weakened (enhanced) in summer (winter) due to colder (warmer) SSTs in the Indian Ocean. Variations in solar insolation are the main drivers for these SST anomalies, verified by very strong temporal anticorrelations between Total Solar Irradiance and All India Monsoon Rainfall in summer monsoon months. The external solar forcing is coupled and overlain by internal climate modes of the ocean (ENSO and Indian Ocean Dipole) with asynchronous intensities and lengths of periods.

In addition, the model simulations have been compared with a relative moisture index derived from paleoclimatic reconstructions based on various proxies and archives in India. In this context, the Lonar record in Central India has been highlighted and evaluated the first time. The simulated annual "Precipitation minus Evaporation" anomalies in comparison to present-day climate are in relative good spatial agreement with the reconstructed moisture index for MWP and LIA climate especially over Central India and the eastern Himalayas.

In order to investigate the interannual monsoon variability with respect to monsoon failures, dry summer monsoon composites for 30-year-long periods of MWP, LIA and REC have been further analyzed. Within dry years of LIA, the summer rainfall over India and the surrounding

oceans is less than in MWP indicating stronger drying conditions due to a stronger summer solar insolation forcing coupled with variations in ENSO. To quantify the ECHAM5 simulated long-term drought conditions within Monsoon Asia, the Palmer Drought Severity Index has been additionally estimated for recent climate showing a strong pattern correlation between global SST anomalies and the Empirical Orthogonal Function variability signal of the drought index, whereas the temporal relationship is weak.

1 Introduction

Based on long-term climate reconstructions derived from various well-dated proxy data (e.g., Borgaonkar et al., 2010; Fleitmann et al., 2007; Liu et al., 2009; Ponton et al., 2012; Prasad et al., 2006) the last Millennium is the best documented historical climate epoch. It can be divided into two major climate periods: the Medieval Warm Period (ca. 900-1350 AD) and the Little Ice Age (ca. 1500-1850 AD) (e.g., Graham et al., 2010; Lamb, 1965; Grove, 1988). Variations in solar insolation coupled with the remote impact of the internal dynamics of climate modes in the oceans like ENSO and Indian Ocean Dipole are some of the major drivers leading to long-term fluctuations in global temperature conditions during the last 1200 years with the occurrence of the characteristic warm and cold periods. These thermal changes show a strong impact on global and regional climate phenomena like monsoons (Polanski et al., 2012), which are primarily formed due to seasonal and latitudinal differences in the incoming solar radiation with effects on the land-sea thermal contrast (Gadgil, 2003; Webster et al., 1998). As consequence, large-scale pressure gradients are generated including strong low-level atmospheric wind circulations (Dallmeyer et al., 2012). Monsoon systems are characterized by a strong spatiotemporal variability from multi-millennial to intraseasonal time scales (Ding, 2007; Lau et al., 2000; Wang, 2006). The Asian Monsoon System is the strongest monsoon system of the world (Clift and Plumb, 2008), which is divided into two strongly non-linear interacting subsystems: the East Asian Monsoon and the Indian Monsoon (Wang et al., 2001) affecting the livelihood of more than 2.5 billion people especially by the increased occurrence and frequency of extreme monsoon rainfall like deficient rainfall events with impacts on meteorological and agricultural drought conditions in recent times (e.g., Krishnan et al., 2009; Shaw and Nguyen, 2011; Ummenhofer et al., 2012). Therefore, the understanding of the large-scale mechanisms and regional spatiotemporal variations leading to extended past monsoon failures (megadroughts) is crucial for improving the Indian Monsoon forecasting and to develop proper mitigation strategies for the future. In this context

a combined multi-proxy-climate model approach, as presented in HIMPAC ("Himalaya: Modern and Past Climates"; http://www.himpac.org) and CADY ("Central Asian Climate Dynamics"; http://www.cady-climate.org) projects, can be used to analyze the past monsoon climate in India within the last Millennium.

Several paleoclimate studies have been already carried out to investigate drought conditions in Asia during the last Millennium as well as in present-day (e.g., Cook et al., 2010; Krishnan et al., 2009; Sinha et al., 2011b) using different multiproxy archives, observation and reanalysis data as well as climate model simulations. For instance based on new tree-ring width reconstructions, Sinha et al. (2011b) postulate episodic and widespread reoccurrences of monsoon megadroughts continued throughout the LIA, which are not clearly related to ENSO variability in the tropical Pacific Ocean as seen in present-day. Moreover, intraseasonal monsoon variability with a "break" spell dominated mode favors reduced precipitation over India along with a southward retreat of the ITCZ (Sinha et al., 2011b) and intensified rainfall over the Himalayan region (Gadgil, 2003). Other studies suggest that the occurrence of wet (India-Pakistan region) and dry (Bay of Bengal region) monsoon signals are in response to shifting atmospheric circulation patterns due to changes in SST and local convection (Mujumdar et al., 2012). The combination of statistical data analysis and/or climate simulations with paleoclimatic reconstruction methods has been performed in several studies (e.g., Hind et al., 2012; Jones et al., 2009; Kleinen et al., 2011; Rehfeld et al., 2012; Sundberg et al., 2012).

The following study describes the monsoon variability and its large-scale physical mechanisms on different time scales with a focus on monsoon failures within the last Millennium for the Medieval Warm Period, the Little Ice Age and the recent climate respectively by an analysis of global climate model simulations with the general circulation model ECHAM5. To get a consistent view of the past climate, paleoclimatic model simulations describe the historical climate on different spatiotemporal scales by consideration of external forcing parameters like solar variations, volcanoes or land cover changes derived from reconstructions. General circulation models of the atmosphere (AGCMs) are often used to simulate the large-scale atmospheric circulation (e.g., Kaspar et al., 2010) and the related monsoon circulation. Owing to the coarse horizontal resolution, global AGCMs are not able to capture regional-scale atmospheric circulation and precipitation processes, which strongly depend on the realistic simulation of the local topography (Polanski et al., 2010). Therefore,

in this study a higher resolved AGCM is used to better resolve the rainfall patterns in orographically induced regions. In addition the model simulations will be compared with paleoclimatic reconstructions based on different proxies and archives in India. In this context the reconstructed climate of the well-dated Lonar record in Central India plays an important role (Anoop et al., 2013; Prasad et al., 2013). Due to its special location in the sensitive Core Monsoon Zone, the site is probably influenced by both monsoon branches: from the Arabian Sea and the Bay of Bengal. Particularly with regard to the long continuously chronology of the last 11000 years, the Lonar site presents a unique possibility for a comparison of long-term climate time series. Therefore, here the evaluation with climate model simulations is introduced and highlighted for the first time.

After a short introduction of the global climate model simulations, the reconstructed relative moisture index and the observation data are presented as well as different climate indices used for this study (section 2). In section 3 the modern spatiotemporal summer monsoon climatology is validated with observation data. Section 4 presents the simulation results for the last Millennium, in which the driving mechanisms for anomalous dry monsoon years are analyzed. Further, the Palmer Drought Severity Index is calculated to quantify the monsoon failures in model data in comparison with tree-ring based drought conditions. In addition, the calculated annual P-E anomalies are compared with paleoclimatic reconstructions based on the moisture index. Finally, concluding remarks summarize the main results (section 5).

2 Model and data

2.1 Global climate model simulations

The general framework (Fig. 1) of the climate model simulations within the HIMPAC and CADY project for the last Millennium encompasses a three step hierarchy of model runs starting from a fully coupled atmosphere-ocean-land surface-biogeochemistry global model (Max Planck Institute for Meteorology Earth System Model (MPI-ESM)) for the entire past Millennium with 1206 model years, a set of different ensemble members and a coarse horizontal resolution (A), an atmosphere-only general circulation model (ECHAM5) in a higher spatial resolution for three time slices with a length of 200 years (B) and a high resolution regional climate model (COSMO-CLM) for 30 year time slices (C). In a first step the MPI-ESM has been analyzed to detect extreme wet and dry summer monsoon rainfall anomalies over India on centennial time scales of about 200 year time periods to simulate

them on a higher spatial resolution with ECHAM5 in a time slice mode. Later the output of the higher resolved global model will be used to identify extreme active and passive monsoon phases within the 200 years and to drive the COSMO-CLM at its lateral and lower boundaries by dynamical downscaling over a domain covering Monsoon Asia, which is beyond the scope of this study and thus will not be shown.

2.1.1 Max Planck Institute for Meteorology Earth System Model (MPI-ESM)

All climate model simulations used in this study are based on the analysis of a set of five ensemble members of the fully coupled MPI-ESM (Jungclaus et al., 2010), which were conducted in the framework of the Integrated Project Millennium (http://www.mad.zmaw.de/service-support/consortium-model-runs/millennium-experiments/index.html) at the Max Planck Institute for Meteorology (MPI). The model includes different components, which are coupled with each other: ECHAM5 (European Centre, HAMburg, version 5) (Roeckner et al., 2003): the general circulation model for the atmosphere (AGCM) and MPIOM (Max Planck Institute Ocean Model) (Marsland et al., 2003): the GCM for the ocean. The dynamical core of ECHAM5 is based on spectral weather prediction models, which have been developed at the ECMWF and modified for climate research at MPI. The MPIOM consists of thermodynamic sea-ice processes and simulates the ocean circulation in response to the atmospheric forcing. ECHAM5 and MPIOM are coupled via the OASIS coupler. Furthermore the ocean biogeochemistry module HAMOCC5 (HAMburg Oceanic Carbon Cycle Model, version 5) (Wetzel et al., 2006) and the land surface scheme JSBACH (Joint Scheme for Biosphere Atmosphere Coupling in Hamburg) (Raddatz et al., 2007) are considered in the MPI-ESM.

The long-term model experiments from Jungclaus et al., 2010 are performed with the MPI-ESM using ECHAM5 in a coarse spectral horizontal resolution of T31 (ca. 3.75° x 3.75° = ca. 380 x 380 km) with 19 irregular vertical levels in hybrid σ-p-coordinates from the surface up to 10 hPa. MPIOM has been run with a horizontal resolution of GR3.0 (ca. 3° x 3°) with 40 vertical levels. An ensemble of five simulations starting from different ocean initial conditions covers the time from 800 to 2005 AD. A set of standard full forcing has been considered in running the model for all ensemble members: a) Solar forcing: Variations in the Total Solar Irradiance (TSI) have been used with a standard increase of 0.1% from the Maunder Minimum (1647-1715 AD) to today sampled by Krivova et al., 2007. Further the 11-yr

activity cycle based on reconstructed sunspot numbers is included. The TSI time series from 800 AD to the Maunder Minimum are reconstructed on the basis of cosmogenic isotope ^{14}C concentrations in tree rings (Solanki et al., 2004). In this study we used the mil0014 member of the E1 ensemble simulations with a weaker solar variation compared to ensemble E2, which has to be considered in the analysis of TSI fluctuations. A solar constant value of 1367 Wm^{-2} is applied (Jungclaus et al., 2010); b) Volcanic forcing: The volcanic effect on the radiation is estimated interactive in the model by using aerosol optical depth (AOD) time series at 0.55 µm and of the effective radius (Crowley et al., 2008); c) Land cover changes: A reconstruction of global agricultural regions and land cover is used to describe the anthropogenic land cover changes (Pongratz et al., 2008) by merging published agriculture maps from 1700 to 1992 AD and a population based approach from 800 to 1700 AD. The maps have a spatial resolution of 0.5° and include 14 vegetation types; d) Orbital forcing: Periodic variations of the Earth's orbit around the sun including short-term fluctuations are represented in ECHAM5 by applying the Variation Seculaires des Orbites Planetaires (VSOP) analytical solution (Bretagnon and Francou (1988) with a determination of the orbit from –4000 to 8000 years with respect to the year 2000; e) Greenhouse gas forcing: The CO_2 concentration is computed interactively within the model. Fossil fuel emissions for the historical period are prescribed after Marland et al. (2003) and the present-day ozone climatology is used from Fortuin and Kelder (1998); f) Aerosol forcing: The climatological background aerosol distribution is based on time independent spatial distributions of tropospheric and stratospheric background aerosols (Tanre et al., 1984) with a maximum AOD of 0.55µm. The data have been interpolated linearly between 1750 and 1850.

The time slice experiments with the atmosphere-alone component ECHAM5 have been run with a higher spectral horizontal resolution of T63 (ca. 1.8° x 1.8° = ca. 180 x 180 km) and 31 vertical model levels. The SST and SIC data have been taken from the coarse resolved model and have been spatially interpolated onto the T63 horizontal grid to initialize the model runs. The same set of full forcing has been also applied for the ECHAM5 simulations to get consistent model runs.

2.1.2 Model simulation setup

Fig. 2 illustrates annual rainfall time series averaged over the All-India-Monsoon-Region from 800-2005 AD for the five different ensemble members of the Millennium experiment

(Jungclaus et al., 2010) using the coarse resolution MPI-ESM. According to the highest temporal correlation of ensemble member mil0014 (0.67) for All India Monsoon Rainfall (AIMR) compared to the ensemble mean, three 200-year long time slices for Medieval Warm Period (MWP; 900-1100 AD), Little Ice Age (LIA; 1515-1715 AD) and Recent Climate (REC; 1800-2000 AD) have been chosen to simulate them with the higher resolved atmosphere-only ECHAM5 model to identify the response of different horizontal resolutions of the atmospheric model component on the simulation of extreme monsoon rainfall events on multidecadal to centennial time scales and to investigate the dynamics and teleconnections leading to these events. The selection of the time slices within the prominent climatic periods for the MWP and LIA has been also done in comparison with the thermal conditions during these periods to identify the most dominant climatic signals within the last 1000 years.

2.2 Data

2.2.1 Reconstructions

The ECHAM5 simulated moisture changes between MWP, LIA and REC are compared with 9 reconstructed paleo-data (Bhattacharya et al., 2007; Chauhan et al., 2000; Denniston et al., 2000; Ely et al., 1999; Kar et al., 2002; Ponton et al., 2012; Prasad et al., 2013 and Sinha et al., 2011a) derived from different archives like lake sediments, peat and stalagmites (see Tab. 1) using various proxies like pollen, isotopes, mineralogy and sedimentology. The archives in the region (76°E-92°E and 16°N-32°N) are influenced by Indian Summer Monsoon (ISM) and Westerlies encompassing the Core Monsoon Zone (CMZ) in Central India as well as the northern Himalayan region (see Fig. 3 for summer). Since the sites in the CMZ are mostly affected by ISM throughout the year, the Himalayan sites show a seasonality in the moisture source origin between summer (ISM) and winter (Westerlies) due to the northward (southward) shift of the ITCZ band in the corresponding summer (winter) season. The annual relative moisture signal from the multiproxy investigations has been translated into a qualitative moisture index for a three-part scale: minus (plus) values indicate drier (wetter) conditions in each 200 year time slice compared to the reference period 1800-2000. “No changes” are marked with zero values.

2.2.2 Observational and reanalysis data

The validation of modern summer monsoon rainfall patterns over land surface regions between ECHAM5 model and gridded observations has been carried out with GPCC6

reanalysis data from Global Precipitation Climatology Centre (Schneider et al., 2011) and the APHRODITE Monsoon Asia (60°E-150°E/15°S-55°N) Gridded Rainfall Data Set (Yatagai et al., 2012) for a present-day period from 1951 – 2000. Both observation data sets have a spatial horizontal resolution of 0.5°.

2.3 Climate indices

In order to quantify the long-term relationship between global teleconnection patterns and the AIMR in summer (JJAS) the temporal correlation between different climate indices and the AIMR has been calculated.

2.3.1 Total Solar Irradiance

The Total Solar Irradiance (TSI) is defined as the amount of the shortwave radiation emitted by the sun with integrated wavelengths (spectra) determined by the sun temperature. Irradiance is defined as the amount of electromagnetic energy incident on a surface per time and area (http://www.ipcc.ch/pdf/glossary/tar-ipcc-terms-en.pdf; http://science.jrank.org). The ECHAM5 calculated annual TSI (Wm^{-2}) value, used in this study, is taken from the "net shortwave incoming solar radiation" model parameter at the top of the atmosphere. The reconstruction of the TSI variations in the driving MPI-ESM has been done by Krivova et al., 2007 and Solanki et al., 2004. In this study, the TSI value has been calculated for summer (JJAS) averaged over the AIMR domain and the 200-yr time slices of MWP, LIA and REC to better compare it with the summer rainfall signals during these periods in that region.

2.3.2 Oceanic Niño Index

The oceanic part of the ENSO phenomenon has been analyzed by calculating the annual Oceanic Niño Index (ONI) from NOAA/NWS/CPC, 2011 based on the SST anomalies in the Niño 3.4 region (120°W - 170°W and 5°S - 5°N) The thresholds for El Niño and La Niña are defined by the following criteria:

El Niño: at least 5 consecutive seasons with an ONI ≥0.5°C

La Niña: at least 5 consecutive seasons with an ONI ≤0.5°C.

2.3.3 Dipole Mode Index

The Dipole Mode Index (DMI) has been calculated by the difference of annual SST anomalies between the tropical western Indian Ocean (50°E - 70°E and 10°S - 10°N) and the tropical southeastern Indian Ocean (90°E - 110°E and 10°S - 0°S). The index oscillates between positive and negative values. A positive (negative) DMI event is characterized by warmer (cooler) than normal SSTs in the western and cooler (warmer) SSTs in the eastern basin (Clark et al., 2003).

2.3.4 All India Monsoon Rainfall

The All India Monsoon Rainfall measures the strength of the Indian Monsoon, which is defined by the summer rainfall anomalies averaged over the homogeneous Indian Peninsular including different sub regions from June to September (http://www.tropmet.res.in). Since the AIMR domain shows a spatial inhomogeneity in rainfall patterns especially on interannual time scale (Conroy and Overpeck, 2011), the results have to be interpreted carefully. However, to get a consistency in that manuscript in accordance with the main objectives within this study, the state-of-the-art entire AIMR domain is used, which has been successfully applied in numerous other ISM studies before (e.g., Krishnan and Sugi, 2003).

2.3.5 Palmer Drought Severity Index

The Palmer Drought Severity Index (PDSI) developed by Palmer, 1965 is one of the best climatological indicators of the prolonged and abnormal periods of moisture deficiency, which can quantify the drought severity over different climates (Wells et al., 2004). The monthly PDSI has been calculated to quantify long-term drought conditions within the ECHAM5 simulations for the period from 1856 to 2000 AD overlapping with the Kaplan SST V2 data provided by the NOAA/OAR/ESRL PSD, Boulder, Colorado, USA from their web site at http://www.esrl.noaa.gov/psd/ for further investigation of the correlation between Sea Surface Temperature Anomalies (SSTA) and droughts over Monsoon Asia. The climatological dataset of available water content from global soil texture and derived water-holding capacities (Webb et al., 2000) has been used for PDSI calculations.

3 Modern summer monsoon climatology -and variability

In order to evaluate the skill of the ECHAM5 simulated spatiotemporal summer monsoon patterns, in a first step the rainfall simulations have been compared with the coarse resolved

MPI-ESM of Millennium Experiment (Jungclaus et al., 2010) as well as with two gridded observed rainfall data sets (Schneider et al., 2011; Yatagai et al., 2012) for a recent time period from 1951 – 2000. The focus is on analyzing the skill of the climate simulations with respect to different horizontal resolutions for past climate studies.

3.1 Spatial rainfall patterns (JJAS)

Compared to GPCC6 the agreement in the climatology and interannual variability of the spatial ISM rainfall patterns over land surface regions, simulated by the higher resolved ECHAM5 model for the period from 1951 – 2000 (not shown), is much better than for the coarse resolved MPI-ESM, which is primary related to the more detailed representation of orographic features in the higher resolved GCM. The coarse model shows a homogeneous rainfall distribution, whereas ECHAM5 T63L31 simulates topography induced rainfall belts more realistically. Due to the characteristic modern ISM circulation with deep convection and orographic uplifting processes, intensive and long-term extended rainfall events prevail especially in the windward of the Western Ghats at the Malabar Coast, at the southern slopes of the Himalayas and in the northern Bay of Bengal, which are relatively well captured by ECHAM5 even if the amount of rainfall is less than in GPCC6. Therefore, the realistic simulation of orography and small scale rainfall patterns respectively is crucial to get a better understanding of changes in rainfall distribution over short horizontal distances in a highly structured relief, which has been achieved by the higher resolved ECHAM5 model.

3.2 Temporal rainfall climatology (JJAS)

The Taylor diagram (Taylor et al., 2001) has been used to compare the simulated and observed temporal summer monsoon rainfall climatology from 1951 – 2000 covering a box over India (0°N - 50°N and 60°E - 120°E). First the higher resolved ECHAM5 model output (T63L31) and the observations have been bilinearly interpolated to the coarser grid of the MPI-ESM (T31L19) before analyzing the data. Fig. 4 shows a good temporal correlation and a small RMSE between the two observations as well as between the two models. The coarser resolved MPI-ESM (D) represents a slightly better agreement with GPCC6 (B) and APHRODITE (A) than ECHAM5 (C) with the increased spatial resolution. The standard deviation of the coarser resolved model is also closer to GPCC6. It is believed that higher spatial resolved simulations can better capture the internal climate variations, which might be one possibility to limit the potential agreement between model simulations. The temporal

correlation of the two climate models and GPCC6 is about 0.6 and the centered RMSE is about 0.5 for MPI-ESM and 0.7 for ECHAM5. We additionally divided the total rainfall of MPI-ESM and ECHAM5 into convective and large-scale precipitation (not shown). The bias in the large-scale precipitation between both model resolutions is less than in the convective precipitation, where ECHAM5 is overestimated. Therefore, the higher RMSE of ECHAM5 is due to the cumulus convection parameterization scheme. However, the interannual variability is much better resolved by ECHAM5.

In general the ECHAM5 model is able to successfully simulate the modern spatiotemporal patterns of summer monsoon rainfall climatology -and variability with respect to observation data, which has been already shown in other state-of-the-art global monsoon modeling studies (e.g., Dallmeyer et al., 2010). Therefore, it can be used for further interpretation of past climate changes in the Indian Monsoon.

4 Climatic change of Indian Monsoon during Last Millennium

4.1 Simulated Rainfall Changes and Comparison with Reconstructions

Changes in the external forcing (e.g., Total Solar Irradiance (TSI), volcanoes or orbital parameters) and in the diabatic heating source have an impact on the circulation and rainfall patterns (Dallmeyer et al., 2010). In Fig. 5 the climatological summer (JJAS; upper panel) and winter monsoon (DJF; lower panel) relative rainfall anomalies are illustrated for the ECHAM5 simulations during the MWP, LIA and REC time slices.

Compared to REC, for the MWP (a) summer months, ECHAM5 simulates less rainfall over most parts of western Central Asia, the northern Arabian Sea, India and the Bay of Bengal and increasing rainfall northeast of this region including the Tibetan Plateau, which is statistical significant. This dipole precipitation pattern is related to regional changes in temperature and circulation. The overall warming signal in MWP is more pronounced north of 30°N and a slight cooling is simulated in the tropics. Therefore, the intensity of temperature gradient and the position of the ITCZ are shifted to the east going along with an enhancement of EASM (not shown). Drier conditions over northern Arabian Sea and Bay of Bengal are connected to lower SSTs in the ocean basins implying a reduction of local convection related to a decreasing moisture convergence, weaker upward motion of moisture and a decreased instability in the vertical column of the troposphere (Polanski et al., 2010). In LIA summer (2) the dipole pattern disappears compared to REC and a slight intensification of

ISM is simulated with increasing rainfall amount over India, the Tibetan Plateau and over the regions influenced by EASM. The LIA is characterized by a summer cooling trend over tropics and a slight warming over northeastern Asia. Therefore, the rainfall changes are more embedded in the large-scale circulation driven by the meridional temperature gradient between the cooler Indian Ocean with the surrounding land surface regions and the warmer northeastern Eurasian continent (not shown). The comparison in (c) verifies the characteristic regional intensification and weakening trends in summer monsoon rainfall between the warmer and cooler time slice.

In the winter months (lower panel) the MWP (a) and LIA (b) show similar spatial rainfall anomalies compared to REC with more simulated rainfall over Indian subcontinent, Tibetan Plateau, the Bay of Bengal and East Asia and less rainfall northern of 35°N especially seen for LIA epoch. The wetter winter conditions during LIA (b) are connected to an enhancement of Westerlies inducing more precipitation events at Himalayan slopes and southern parts. The comparison between MWP and LIA (c) illustrates the drier winter in MWP over India and the surrounding ocean basins and wetter winter conditions eastern of that region. These changes are related to an intensification of Westerlies over Tibetan Plateau going along with the northern shift and weakening of the Siberian High (not shown).

In general the climatological summer- and winter monsoon comparison between MWP and LIA indicates that less rainfall is simulated over India and southwestern regions and more rainfall is calculated over Central Asia during the warmer climate, which are determined by regional and large-scale dynamics. In order to quantify the dynamical relationship between AIMR in summer with external solar forcing and internal feedbacks based on different climate modes (see section 2.3), the temporal correlation coefficients have been calculated among the different indices for the three simulated time slices. Before applying the calculation for the ECHAM5 data, the different indices have been validated for present-day with observation data (not shown). The solar forcing, defined by the TSI, is the main driver for summer monsoon rainfall with a strong anticorrelation of - 0.95 (- 0.94 and - 0.95) for MWP (LIA and REC), which is statistically significant at a 99% confidence level (see Tab. 2). Due to various interacting physical mechanisms and feedbacks on different spatio-temporal dimensions, we assume a complex and overlaying non-linear process that impacts the negative relationship between solar irradiance and Indian rainfall in summer months not locally but more under a large-scale aspect, which has been already discussed in other studies

(Meehl et al., 2009). An overall warming (cooling) period like the prominent MWP (LIA) is not solely leading to a homogeneous warming (cooling) over all regions, but more to a regionalization and inhomogeneity due to overlaying internal factors. Secondly, local effects of solar forcing (higher TSI leads to more rainfall and vice versa) are mostly suppressed and dominated by large-scale processes between the atmosphere and the ocean (e.g., evaporation and horizontal advection of moisture based on a changed atmospheric circulation). Further it has to be considered that the total solar irradiance in the model is influenced by an orbital-scale change and short-term 11-yr solar fluctuations, which are more important for the interpretation of these mechanisms since the long-term changes don't show any significant fluctuation and trend within the 200-yr time slices between MWP and REC and thus can be neglected in the analysis of centennial-scale rainfall composites and its external forcing. For a better understanding of these mechanisms, we additionally calculated the spatial distribution of TSI anomalies. The climatological 200-yr averaged spatial TSI differences "MWP minus REC" (not shown) indicate a mostly zonally orientated pattern with an increase of solar irradiance in a belt from the central Arabian Sea, central and southern India, the Bay of Bengal and southeastern Asia corresponding to drier conditions. Lower TSI values (not shown) are simulated from eastern Himalayas, over southwestern Tibetan Plateau to eastern China in correspondence with wetter conditions. In LIA epoch the respective spatial TSI anomalies compared to REC show again an increase from the Arabian Sea over southern India, the Bay of Bengal and southeastern Asia, but a more pronounced decrease from northern India over the Ganga Plains towards the eastern regions as well as a slightly increase over the Tibetan Plateau. Especially the southward shift of the positive TSI anomaly pattern over India and thus the stronger gradient between southern and northern India including the surrounding ocean basins can trigger the enhancement of the moisture penetration towards the Ganga Plains resulting in higher rainfall in LIA than in MWP. We conclude, that related to the large-scale aspect, a higher (lower) solar shortwave irradiance at the top of the atmosphere over Indian land surface (here referred as solar activity of the 11-yr cycle) leads to a mid- and lower tropospheric warming (cooling) of the corresponding areas, but as the insolation changes are spatially inhomogeneous over India, a spatial inhomogeneity in temperature, atmospheric circulation and rainfall patterns are simulated. The different thermal evolutions result in a weakening (amplification) of the monsoonal-driving large-scale meridional temperature gradient between the ocean and the land surface with a reduction (intensification) of the cross-equatorial monsoonal winds at the lower troposphere. This is followed by a

decrease (increase) and a shift in the position of the monsoonal heat low with the corresponding deep convection area over northwestern India embedded in the broad ITCZ band, which is shifting south - eastward (north - westward). The calculated SLP fields underline the changes in atmospheric circulation (not shown), even if the signals are not as pronounced and significant. Finally a weaker (stronger) ISM due to the rainfall intensity can be identified. The 2m-air temperature anomalies are mostly influenced by the rainfall strength via negative moisture-temperature feedbacks. Higher (lower) rainfall amounts are associated to evaporation cooling (warming). The external forcing is overlain by internal variability modes of the ocean (e.g., ENSO and IOD) with asynchronous intensities and lengths of periods shown by anticorrelations of - 0.63 (- 0.61 and - 0.66) for the ONI in MWP (LIA and REC) and - 0.59 (- 0.47 and - 0.56) for the DMI in MWP (LIA and REC) (see Tab. 2). Since ENSO has a strong impact on the interannual rainfall variations over India in the past Millennium (e.g., Sinha et al., 2011a, b) leading to extreme wet (dry) conditions, we will emphasize more on the AIMR-El Niño linkage in the analysis of 30-yr long dry summer monsoon composites (see section 4.2).

Moisture changes during the Last Millennium have been described by paleoclimatic reconstructions based on a relative moisture index using different archives and proxies (Anoop et al., 2013; Bhattacharya et al., 2007; Chauhan et al., 2000; Denniston et al., 2000; Ely et al., 1999; Kar et al., 2002; Ponton et al., 2012; Prasad et al., 2013) (Fig. 6). The figure compares the ECHAM5 simulated normalized annual "Precipitation minus Evaporation" (P-E) anomalies and the reconstructed paleoclimatic moisture index between MWP, LIA and REC. Since the driving model simulations of the coarse resolved Millennium Experiment show a significant long-term increasing trend in the solar irradiance and the Meridional Overturning Circulation (MOC) in the Atlantic Basin for the last 100 years (Zanchettin et al., 2010), the ECHAM5 simulated P-E time series for REC had been detrended before the comparison with the P-E anomalies of the other time slices to eliminate the long-term climate signal.

In the MWP (a) the model simulates drier (wetter) conditions over Central India (Himalayas) compared to REC, which can be also captured by the reconstructed moisture index with same signs of qualitative moisture changes. In spite of the missing statistical significance of P-E anomalies in these regions, a good spatial agreement between model and proxy data can be evaluated. The LIA epoch (b) shows a similar spatial distribution of the simulated annual P-E anomalies with drier (wetter) conditions in the CMZ (Himalayan region) compared to REC.

Especially the sites at Lonar and Paradise Lake indicate a consistent agreement in the signals for both periods. Compared to LIA, the modeled MWP is much drier in Central India and in the western and central Himalayas (see Fig. 6c) than in the reconstructions showing opposite signs in the moisture signal except for Paradise Lake in the eastern Himalayas, where model and reconstruction agree for the wetter conditions in MWP (see Fig. 6c).

The model-proxy disagreement between MWP and LIA is likely related to the external forcing or to model biases due to physical parameterization of ECHAM5 model (e.g., Weber and Quaas, 2012). The study from Dallmeyer et al. (2012) further suggests the importance of extending the analysis period of monsoon climate change to other seasons. The paleoclimate moisture reconstructions cannot be used as single indicator for the ISM intensity and the related precipitation. It is assumed that the orbital variations lead to an inhomogeneous seasonal insolation distribution and impacts the rainfall throughout the year. Therefore, the reconstructed moisture signals should not be correlated and explained with variations in summer insolation (Dallmeyer et al., 2012). Since the reconstructed moisture signal is annual based, this analysis cannot be carried out within this study. Further research has to be done in isolating the seasonality in reconstructions.

4.2 Dry Summer Monsoon Composites

4.2.1 Simulated Rainfall Anomalies

In order to investigate the interannual summer monsoon (JJAS) variability of the last Millennium with a focus on extreme rainfall events and its linkage to ENSO, three 30-years-long strong (wet) and weak (dry) monsoon composites for every 200-year time slices of MWP, LIA and REC have been selected and compared with each other regarding their characteristic rainfall anomalies and regional as well as large-scale dynamical drivers. The focus of the following analysis is on weak rainfall events leading to significant monsoon failures (droughts). The selection of the anomalous dry summer monsoon years (MWP: 992-1022 AD, LIA: 1633-1663 AD and REC: 1913-1943 AD) has been done by the calculation of ECHAM5 time series averaged over the AIMR region (not shown). Fig. 7 illustrates the ECHAM5 simulated anomaly composites of summer monsoon rainfall (upper panel) and 2m-air-temperature (lower panel) for “MWP minus REC” (a), “LIA minus REC” (b) and “MWP minus LIA” (c).

During weak monsoon years of MWP and LIA the spatial large-scale pattern of the precipitation differences are quite similar. This is an indication that the driving mechanisms of extreme dry summer monsoon rainfall are similar in both periods compared to recent climate. Particularly, similar regional patterns of rainfall anomalies are simulated over the Himalayas and Tibetan Plateau (wetter), central, southern and northeastern India including northern Bay of Bengal (drier). In contrast, northwestern India and the northern Arabian Sea show clear opposite and statistical significant summer rainfall signals between MWP (wetter) and LIA (drier), which are related to changes in the atmospheric circulation and temperatures. These changes can be attributed to a similar shift of the West Pacific Subtropical High during 2010 flooding in Pakistan with suppressing of convection around Bay of Bengal and sustaining the rainfall activity over northwestern India and Pakistan, strongly influenced by internal modes of the Ocean like La Niña and IOD (Mujumdar et al., 2012). In MWP the temperature gradient between Indian Ocean and Eurasian land surface is higher due to warmer temperature anomalies especially over central India and the continental regions north of Arabian Sea (+0.5K) compared to LIA (see Fig. 7c). The SST changes over the Indian Ocean are another important driver for the modified atmospheric circulation and rainfall patterns in dry monsoon years between MWP and LIA (not shown), which also influence the local convection. The positive anomalies in vertical velocity at 500 hPa (not shown) represent the regions with strongest convective activity, which are associated with a strong moisture convergence as well as a strong upward motion in the middle troposphere. This relationship is shown for both MWP and LIA. In MWP the strongest convective activity occurs over India and the Arabian Sea, whereas the convection is reduced over these parts in LIA as a result of shifted atmospheric circulation patterns. Changes in the distribution of rainfall anomalies are associated to shifting regional atmospheric circulation patterns driven by modified regional SST anomalies in the Indian Ocean and due to changes in external forcing and internal feedbacks of the surrounding Oceans (see also section 4.1). As already discussed for the centennial scale composites, the dominant driver for monsoon precipitation are solar variations, which can be also verified for the 30-yr long dry monsoon composites. The temporal correlation between AIMR and TSI in summer months is quite high (e.g., -0.98 for MWP) with a statistical significance at 99% confidence level. According to Table 2 we calculated the temporal correlation coefficients between the different forcing factors and the AIMR considering the uncertainties by using shorter time scales for testing the significance. Compared to Table 2 the ENSO phenomenon shows a stronger impact on the rainfall

variations on interannual to decadal time scale (e.g., -0.70 for MWP at 99% statistical confidence level) than on centennial time scale. The model based correlation between DMI and AIMR tends towards zero, which can be related to some internal model problems, but as suggested in other studies (e.g., Mujumdar et al., 2012) we assume an additional strong effect of the Indian Ocean SST Variability on interannual dry monsoon conditions. Summarizing, the mechanisms leading to the inhomogeneous distribution of simulated rainfall anomalies during dry years of MWP and LIA are mostly related to a) large-scale air-sea feedbacks of periodic El Niño/La Niña events with a shifting Walker circulation leading to a weaker (stronger) ISM and less (more) rainfall, but these drier (wetter) conditions are b) modified regionally via different non-linear feedbacks (e.g., internal SST variability in the Indian Ocean and regional changes in the atmospheric circulation via shifting of the ITCZ position) further expressed by significant wetter (drier) conditions in the Indo-Pakistan region in MWP (LIA). The temperature signals shown for the dry composites indicate a more pronounced response of precipitation than vice versa. Warm (cold) anomalies in the 2m-air temperature patterns are associated to evaporation warming (cooling) due to less (more) rainfall and weaker (stronger) cloudiness in the region as already discussed for the climatological 200-yr anomalies. Finally it can be identified, that the convection is driven by large-scale moisture advection from the Indian Ocean and a strong upward motion of water vapor over land related to enhanced instability and moisture convergence, which has been already analyzed in previous studies (e.g., Bhalme et al., 1980; Krishnan et al., 2003; Polanski et al., 2010).

4.2.2 Palmer Drought Severity Index and Global SST Anomalies

Further the characteristic rainfall patterns in dry monsoon years have been correlated to global SST anomalies by using Empirical Orthogonal Function (EOF) Analysis to quantify the relationship between monsoon failures (droughts) on interannual time scale and global internal variability modes of the Oceans. According to that, the EOF/PC1 and EOF/PC4 of the PDSI (see also chapter 2.3.6) have been calculated within the Monsoon Asia region for the 200-year-long ECHAM5 present-day simulation (REC) from 1800-2000 AD and later correlated with global SST anomalies from Kaplan SST V2 data for pre- and summer monsoon (MAMJJA) and winter monsoon (DJF) season between 1856 and 2000 AD. The simulation of the broad-scale monsoon failure events with robust long-term modes of spatiotemporal variability can provide deeper insights into the dynamics of Indian monsoon variability (Cook et al., 2010). Two of the EOF modes are highlighted in Fig. 8. The leading

pattern accounts for 15.75% of the total field variability. Dominant same-sign loadings are detected over India, South and Southeast Asia with opposite sign loadings over Tibetan Plateau, northern Pakistan, Pamir and Tien-Shan Mountains, which are in well agreement with the DEOF1 of the reconstructed PDSI from Cook et al., 2010. It indicates the simulated dipole rainfall patterns in dry monsoon years between India and Tibetan Plateau seen especially in LIA. Moreover the temporal expansion of this mode (PC1) correlated well with the hemispherically SST anomalies of interdecadal variability in the Pacific Ocean, seen also in Cook et al., 2010. The late-20th century trend toward drier conditions and weaker monsoons over India and Southeast Asia (see Fig. 8) can be explained by similar mechanisms leading to droughts in MWP and LIA. The EOF4 pattern accounts for 4.5% of the total field variance with strong positive loadings over China and northeastern Asia and negative loadings over India. The PC4 of this mode is positively correlated with Indian Ocean SST anomalies, which are related to the DMI and tends to more positive PDSI values during the last 200 years. The ENSO – PDSI relationship in the ECHAM5 simulation is relatively weak (not shown), whereas the internal dynamics of IOD is more pronounced.

5 Conclusions

The general circulation model ECHAM5 has been used to simulate the Indian Monsoon Variability within the last Millennium. The focus has been on 200-year-long time slices of the Medieval Warm Period (900-1100 AD), the Little Ice Age (1515-1715 AD) and the recent climate (1800-2000 AD). The evaluation of spatiotemporal monsoon patterns with present-day observation data is in agreement with other state-of-the-art monsoon modeling studies. Due to the better horizontal resolution of the ECHAM5 model, the rainfall patterns especially in the orographic regions can be captured more realistically. However, high resolution regional climate models are necessary as an additional tool to improve the skill for the simulation of small scale processes in comparison with observed data.

The centennial scale rainfall changes have been simulated and compared for MWP and LIA in comparison with the recent climate. ECHAM5 calculated a weakening (enhancement) in summer (winter) monsoon rainfall due to colder (warmer) SSTs in the Indian Ocean. Variations in the external solar insolation are the main drivers for these SST anomalies, shown by very strong temporal anticorrelations of - 0.95 (- 0.94 and - 0.94) for MWP (LIA and REC) between the Total Solar Irradiance and the All-India-Monsoon-Rainfall in the

summer monsoon months. Due to various interacting physical mechanisms and feedbacks on different spatio-temporal dimensions, a complex and overlaying non-linear process affects the negative relationship between solar irradiance and Indian rainfall in summer months not locally but more under a large-scale aspect. The local effects of solar forcing (higher TSI leads to more rainfall and vice versa) are mostly suppressed and dominated by large-scale processes between the atmosphere and the ocean (e.g., evaporation and horizontal advection of moisture based on a changed atmospheric circulation). Related to that large-scale aspect, a higher (lower) solar shortwave irradiance at the top of the atmosphere over Indian land surface leads to a mid- and lower tropospheric warming (cooling) of the corresponding areas, but as the insolation changes are spatially inhomogeneous over India, a spatial inhomogeneity in temperature, atmospheric circulation and rainfall patterns are simulated. The different thermal evolutions result in a weakening (enhancement) of the monsoonal-driving large-scale meridional temperature gradient between the Ocean and the land surface with a reduction (intensification) of the cross-equatorial monsoonal winds at the lower troposphere. This is followed by a decrease (increase) and a shift in the position of the monsoonal heat low with the corresponding deep convection area over northwestern India embedded in the ITCZ, which is shifting south - eastward (north - westward). Finally a weaker (stronger) ISM due to the rainfall intensity can be identified. The 2m-air temperature anomalies are mostly influenced by the rainfall strength via negative moisture-temperature feedbacks. Higher (lower) rainfall amounts are associated to evaporation cooling (warming). The external solar forcing is further coupled and overlain by internal climate modes of the Ocean shown by anticorrelations of - 0.63 (- 0.61 and - 0.66) for the ONI in MWP (LIA and REC) and - 0.59 (- 0.47 and - 0.56) for the DMI in MWP (LIA and REC) with asynchronous intensities and lengths of periods.

In addition, a qualitative comparison of the simulated annual P-E changes with paleoclimatic reconstructions based on a moisture index has been carried out for the MPW and LIA according to REC. In this context, the well-dated and long chronology of the Lonar record has been highlighted and compared for the first time with model data. For MWP and LIA there is a good spatial agreement between the model simulation and the reconstructed moisture signal especially for Central India and the eastern Himalayas. However, more sites and higher resolved climate model simulations have to be considered in the analysis for an improved

model-proxy comparison with respect to the inhomogeneities in the spatial rainfall distribution and the reconstruction-inherent uncertainties of proxy data.

In order to investigate the interannual summer monsoon (JJAS) variability of the last Millennium with a focus on extreme rainfall events, three 30-years-long strong (wet) and weak (dry) monsoon composites for every 200-year time slices of MWP, LIA and REC have been selected and compared with each other regarding their characteristic rainfall anomalies and regional and large-scale dynamical drivers. The focus has been on weak rainfall events leading to significant monsoon failures (droughts). During weak monsoon years of MWP and LIA the spatial large-scale pattern of the precipitation differences are quite similar indicating similar driving mechanisms of extreme dry summer monsoon rainfall in both periods compared to recent climate. Particularly, similar regional patterns of rainfall anomalies are simulated over the Himalayas and Tibetan Plateau (wetter), central, southern and northeastern India including northern Bay of Bengal (drier). In contrast, northwestern India and the northern Arabian Sea show opposite summer rainfall signals between MWP (wetter) and LIA (drier), which are related to changes in atmospheric circulation and temperatures. In MWP the temperature gradient between Indian Ocean and Eurasian land surface is higher due to warmer temperature anomalies especially over central India and the continental regions north of Arabian Sea (+0.5K) compared to LIA. Changes in the distribution of rainfall anomalies can be attributed to shifting regional atmospheric circulation patterns driven by modified regional SST anomalies in the Indian Ocean and due to changes in external forcing and internal feedbacks of the surrounding Oceans. The dominant drivers of summer monsoon rainfall variability are variations in the Total Solar Irradiance with high temporal anticorrelations of -0.98, overlapped by nonlinear feedbacks of the oceanic internal climate modes. The ENSO phenomenon has a stronger internal feedback on the interannual rainfall anomalies than the DMI with a temporal anticorrelation of - 0.70.

Furthermore the characteristic rainfall patterns during years of weak monsoon activity have been correlated to global SST anomalies by using EOF Analysis to quantify the relationship between droughts on interannual time scale and global internal variability modes of the Oceans for the present-day simulation from 1800-2000 AD. Dominant same-sign loadings are detected over India, South and Southeast Asia with opposite sign loadings over Tibetan Plateau, northern Pakistan, Pamir and Tien-Shan Mountains, which are in well agreement with the DEOF1 of the reconstructed PDSI from Cook et al., 2010. Moreover the temporal

expansion of this mode (PC1) correlated well with the hemispherically SST anomalies of interdecadal variability in the Pacific Ocean, seen also in Cook et al., 2010.

Acknowledgements

This research was supported and funded by the DFG research group FOR 1380 "HIMPAC – Himalaya Modern and Past Climates" and the BMBF joint research project "CADY – Central Asian Climate Dynamics". The authors thank the individual HIMPAC and CADY teams for permanent support and fruitful discussions, especially Daniel J. Befort for providing a figure. Further we thank Dr. Raghavan Krishnan and Dr. Milind Mujumdar from Indian Institute of Tropical Meteorology (IITM), Pune for enhanced collaboration and interesting discussions within HIMPAC and for their hospitality during a research stay at IITM. The MPI-ESM data from Millennium Experiment had been supplied by the Max Planck Institute for Meteorology (MPI-M) Hamburg. The authors thank Dr. Johann H. Jungclaus, MPI-M Hamburg for MPI-ESM data from Millennium-Experiment and Dr. Stephan J. Lorenz, MPI-M Hamburg for many helpful advices in SST interpolation and running ECHAM5 model. Finally we acknowledge the critical comments of XXX anonymous reviewers, who improved and clarified the manuscript.

References

Anoop, A., Prasad, S., Plessen, B., Naumann, R., Gaye, B., Basavaiah, N., Menzel, P., Weise, S., and Brauer, A.: Palaeoenvironmental implications of evaporative Gaylussite crystals from Lonar Lake, Central India, Journal of Quaternary Science (in press), 2013.

Bhalme, H. N., and Mooley, D. A.: Large-scale Droughts/Floods and Monsoon Circulation, Monthly Weather Review, 108, 1197-1211, 1980.

Bhattacharya, A, Sharma, J., Shah, S. K., and Chaudhary, V.: Climatic changes during the last 1800 yrs BP from Paradise Lake, Sela Pass, Arunachal Pradesh, Northeast Himalaya, Current Science, 93 (7), 983-987, 2007.

Borgaonkar, H. P., Sikdera, A. B., Rama, S., and Panta, G. B.: El Niño and related monsoon drought signals in 523-year-long ring width records of teak (*Tectona grandis L. F.*) trees from south India, Paleogeography, Paleoclimatology, Paleoecology, 285, 74-84, 2010.

Bretagnon, P., and Francou, G.: Planetary theories in rectangular and spherical variables – VSOP 87 solutions, Astron. Astrophys., 202, 309-315, 1988.

Chauhan, M.S, Mazari, R. K., and Rajagopalan, G.: Vegetation and climate in upper Spiti region, Himachal Pradesh during late Holocene, Current Science, 79 (3), 373-377, 2000.

Clark, C. O., Webster, P. J., and Cole, J.: Interdecadal variability of the relationship between the Indian Ocean zonal mode and East African coastal rainfall anomalies, Journal of Climate 16, 548–554, 2003.

Clift, P. D., and Plumb, R. A.: The Asian monsoon: causes, history and effects, Cambridge University Press, Cambridge, 2008.

Conroy, J. L., and Overpeck, J. T.: Regionalization of Present-Day Precipitation in the Greater Monsoon Region of Asia, Journal of Climate, 24, 4073-4095, doi: http://dx.doi.org/10.1175/2011JCLI4033.1, 2011.

Cook, E. R., Anchukaitis, K. J., Buckley, B. M., D'Arrigo R. D., Jacoby, G. C., and Wright, W. E.: Asian Monsoon Failure and Megadrought During the Last Millennium, Science, 328, 486-489, 2010.

Crowley, T. J., Zielinski, G., Vinther, B., Udisti, R., Kreutz, K., Cole-Dai, J., and Castellano, J.: Volcanism and the Little Ice Age, PAGES Newsletter, 16, 22-23, 2008.

Dallmeyer, A., Claussen, M., and Otto, J.: Contribution of oceanic and vegetation feedbacks to Holocene climate change in monsoonal Asia, Climate of the Past, 6 (2), 195-217, 2010.

Dallmeyer, A., Claussen, M., Wang, Y., and Herzschuh, U.: Spatial variability of Holocene changes in the annual precipitation pattern: a model-data synthesis for the Asian monsoon region, Climate Dynamics, 39, 18 pp., doi: 10.1007/s00382-012-1550-6, 2012.

Denniston, R.F., and Gonzalez, L. A.: Speleothem Evidence for Changes in Indian Summer Monsoon Precipitation over the Last ~2300 Years, Quaternary Research, 53, 196-202, 2000.

Ding, Y. H.: The variability of the Asian summer monsoon, Journal of Meteorological Society Japan, 85, 21-54, 2007.

Ely, L. L., Enzel, Y., Baker, V. R., Kale, V. S., and Mishra, S.: Changes in the magnitude and frequency of late Holocene monsoon floods on the Narmada River, central India, Geological Society of America Bulletin, 108 (9), 1134-1148, 1996.

Fleitmann, D., Burns, S. J., Mangini, A., Mudelsee, M., Kramers, J., Villa, I., Neff, U., Subbary, A.-A., Buettner, A., Hippler, D., and Matter, A.: Holocene ITCZ and Indian monsoon dynamics recorded in stalagmites from Oman and Yemen (Socotra), Quaternary Sciences Reviews, 26, 170-188, 2007.

Fortuin, J. P. F., and Kelder, H.: An ozone climatology based on ozone sonde and satellite measurements, J. Geophys. Res., 103, 31709-31734, 1998.

Gadgil, S.: The Indian monsoon and its variability, Annual Review of Earth and Planetary Sciences, 31, 429-467, 2003.

Graham, N. E., Ammann, C. M., Fleitmann, D., Cobb, K. M., and Luterbacher, J.: Support for global climate reorganization during the „Medieval Climate Anomaly“, Climate Dynamics, 37, 1217-1245, doi: 10.1007/s00382-010-0914-z, 2010.

Grove, J. M.: The Little Ice Age, Menthuen, London, 1988.

Hind, A., Moberg, A., and Sundberg, R.: Statistical framework for evaluation of climate model simulations by use of climate proxy data from the last millennium – Part 2: A pseudo-proxy study addressing the amplitude of solar forcing, Climate of the Past, 8, 1355-1365, 2012.

Jones, P.D., Briffa, K.R., Osborn, T.J., Lough, J.M., van Ommen, T.D., Vinther, B.M., Luterbacher, J., Wahl, E.R., Zwiers, F.W., Mann, M.E., Schmidt, G.A., Ammann, C.M., Buckley, B.M., Cobb, K.M., Esper, J., Goosse, H., Graham, N., Jansen, E., Kiefer, T., Kull, C., Küttel, M., Mosley-Thompson, E., Overpeck, J.T., Riedwyl, N., Schulz, M., Tudhope, A.W., Villalba, R., Wanner, H., Wolff, E., and Xoplaki, E.: High-resolution paleoclimatology of the last millennium: a review of current status and future prospects, The Holocene, 19, 1, 3-49, 2009.

Jungclaus, J. H., Lorenz, S. J., Timmreck, C., Reick, C. H., Brovkin, V., Six, K., Segschneider, J., Giorgetta, M. A., Crowley, T. J., Pongratz, J., Krivova, N. A., Vieira, L. E., Solanki, S. K., Klocke, D., Botzet, M., Esch, M., Gayler, V., Haak, H., Raddatz, T., Roeckner,

E., Schnur, R., Widmann, H., Claussen, M., Stevens, B., and Marotzke, J.: Climate and carbon-cycle variability over the last millennium, Climate of the Past 6, 723–737, 2010.

Kar, R., Ranhotra, P. S., Bhattacharyya, A., and Sekar, B.: Vegetation vis-a-vis climate and glacial fluctuations of the Gangotri glacier since the last 2000 years, Current Science, 82 (3), 347-351, 2002.

Kaspar, F., Prömmel, K., and Cubasch, U.: Impacts of tectonic and orbital forcing on East African climate: a comparison based on global climate model simulations, International Journal of Earth Sciences, 99, 7, 1677-1686, 2010.

Kleinen, T., Tarasov, P., Brovkin, V., Andreev, A., and Stebich, M.: Comparison of modeled and reconstructed changes in forest cover through the past 8000 years: Eurasian perspective, The Holocene, 21, 723-734, 2011.

Krishnan, R., and Sugi, M.: Pacific decadal oscillation and variability of the Indian summer monsoon rainfall, Climate Dynamics, 21, 233-242, doi: 10.1007/s00382-003-0330-8, 2003.

Krishnan, R., Mujumdar, M., Vaidya, V., Ramesh, K. V., and Satyan, V.: The abnormal Indian summer monsoon of 2000, Journal of Climate, 16, 1177-1194, 2003.

Krishnan, R., Kumar, V., Sugi, M., and Yoshimura, J.: Internal feedbacks from monsoon-midlatitude interactions during droughts in the Indian summer monsoon, Journal of Atmospheric Sciences, 66, 553-578, 2009.

Krivova, N. A., Balmaceda, L., and Solanki, S. K.: Reconstruction of solar total irradiance since 1700 from the surface magnetic flux, Aston. Astrophys., 467, 335-346, 2007.

Lamb, H. H.: The early medieval warm epoch and its sequel, Paleogeography, Paleoclimatology, 1, 13-37, 1965.

Lau, K. M., Kim, K. M., and Yang, S.: Dynamical and boundary forcing characteristics of regional components of the Asian summer monsoon, Journal of Climate, 13, 2461-2482, 2000.

Liu, X., Dong, H., Yang, X., Herzschuh, U., Zhang, E., Stuut, J.-B. W., and Wang, Y.: Late Holocene forcing of the Asian winter and summer monsoon as evidenced by proxy records from the northern Qinghai-Tibetan Plateau, Earth and Planetary Science Letters, 280 (1), 276-284, 2009.

Marland, G., Boden, T. A., and Andres, R. J.: 2003: Global, regional and national emissions, in: Trends: a compendium of data on global change. Carbon Dioxide Information Center, Oak Ridge National Laboratory, US Department of Energy, Oak Ridge, TN.

Marsland, S. J., Haak, H., Jungclaus, J. H., Latif, M., and Röske, F.: The Max-Planck-Institute global ocean/sea ice model with orthogonal curvilinear coordinates, Ocean Modelling 5 (2), 91–127, 2003.

Meehl. G. A., Arblaster, J. M., Matthes, K., Sassi, F., and van Loon, H.: Amplifying the Pacific Climate System Response to a Small 11-Year Solar Cycle Forcing, Science, 325, 1114-1118, doi: 10.1126/science.1172872, 2009.

Mujumdar, M., Preethi, B., Sabin, T. B., Karumuri, A., Saeed, S., Pai, D. S., and Krishnan, R.: The Asian summer monsoon response to the La Niña event of 2010, Meteorological Applications, 9, 216-227, doi: 10.1002/met.1301, 2012.

NOAA/NWS/CPC: Oceanic Nino Index. NOAA National Weather Service, Center for Climate Prediction, 5200 Auth Road, Camp Springs, Maryland 20746, USA, http://www.cpc.ncep.noaa.gov/products/analysis_monitoring/ensostuff/ensoyears.shtml, 2011.

NOAA/OAR/ESRL PSD: Kaplan SST V2 data, Boulder, Colorado, USA, http://www.esrl.noaa.gov/psd/ (last access: 5.February 2013), 1998.

Palmer, W. C.: Meteorological drought, U.S. Weather Bureau, Res. Pap., No. 45, Washington D.C., USA, 58 pp., 1965.

Polanski, S., Rinke, A., and Dethloff, K.: Validation of the HIRHAM-Simulated Indian Summer Monsoon Circulation, Advances in Meteorology, Vol. 2010, 14 pp. doi:10.1155/2010/415632, 2010.

Polanski, S., Rinke, A., Dethloff, K., Lorenz, S. J., Wang, Y., and Herzschuh, U.: Simulation of the mid-Holocene Indian Summer Monsoon Circulation with a Regional Climate Model, The Open Atmospheric Science Journal, 6, 42-48, doi:10.2174/1874282301206010042, 2012.

Pongratz, J., Reick, C. H., Raddatz, T., and Claussen, M.: A Reconstruction of global agricultural areas and land cover for the last millennium, Global Biogeochem. Cy., 22, GB3018, doi: 10.1029/2007GB003153, 2008.

Ponton, C., Giosan, L., Eglinton, T. I., Fuller, D. Q., Johnson, J. E., Kumar, P., and Collett, T. S.: Holocene aridification of India, Geophysical Research Letters, 39, L03704, doi:10.1029/2011GL050722, 2012.

Prasad, S., and Enzel, Y.: Holocene paleoclimates of India, Quaternary Research, 66 (3), 442-453, 2006.

Prasad, S., Anoop, A., Riedel, N., Sarkar, S., Menzel, P., Basavaiah, N., Krishnan, R., Fuller, D., Plessen, B., Gaye, B., Röhl, U., Wilkes, H., Sachse, D., Sawant, R., and Stebich, M.: Holocene Monsoon Megadroughts from high resolution Lonar lake, central India (unpublished data, last update: 10.5.13).

Raddatz, T. J., Reick, C. H., Knorr, W., Kattge, J., Roeckner, E., Schnur, R., Schnitzler, K.-G., Wetzel, P., and Jungclaus, J. H.: Will the tropical land biosphere dominate the climate-carbon cycle feedback during the twenty-first century?, Climate Dynamics 29 (6), 565–574, 2007.

Rehfeld, K., Breitenbach, S. F. M., Marwan, N., and Kurths, J.: Late Holocene Asian Summer Monsoon dynamics from small but complex networks of paleoclimate data, Climate Dynamics, 39, 17 pp., doi: 10.1007/s00382-012-1448-3, 2012.

Roeckner, E., Bäuml, G., Bonaventura, L., Brokopf, R., Esch, M., Giorgetta, M., Hagemann, S., Kirchner, I., Kornblueh, L., Manzini, E., Rhodin, A., Schlese, U., Schulzweida, U., and Tompkins, A.: The atmospheric general circulation model ECHAM 5 PART 1: Model description, Tech. rep., Max-Planck-Institute for Meteorology, Bundesstr. 53, 20146 Hamburg, Germany, 2003.

Schneider, U., Becker, A., Finger, P., Meyer-Christoffer, A., Rudolf, B., and Ziese, M.: GPCC Full Data Reanalysis Version 6 at 0.5°: Monthly Land-Surface Precipitation from Rain-Gauges built on GTS-based and Historic Data, Global Precipitation Climatology Centre, Deutscher Wetterdienst, Offenbach (Main), doi:10.5676/DWD_GPCC/FD_M_V6_050, 2011.

Shaw, R., and Nguyen, H.: Droughts in Asian Monsoon Region, Community, Environment and Disaster Risk Management, 8, Emerald Books, Kyoto University, Kyoto, Japan, UK, 2011.

Sinha, A., Berkelhammer, M., Stott, L., Mudelsee, M., Cheng, H., and Biswas, J.: The leading mode of Indian Summer Monsoon precipitation variability during the last millennium, Geophysical Research Letters, 38, L15703, doi:10.1029/2011GL047713, 2011a.

Sinha, A., Stott, L., Berkelhammer, M., Cheng, H., Lawrence Edwards, R., Buckley, B., Aldenderfer, M., and Mudelsee, M.: A global context for megadroughts in monsoon Asia during the past millennium, Quaternary Science Reviews, 30, 47-62, 2011b.

Solanki, S. K., Usoskin, I. G., Kromer, B., Schuessler, M., and Beer, J.: Unusual activity of the Sun during recent decades compared to the previous 11000 years, Nature, 431, 1084-1087, 2004.

Sundberg, R., Moberg, A., and Hind, A.: Statistical framework for evaluation of climate model simulations by use of climate proxy data from the last millennium – Part 1: Theory, Climate of the Past, 8, 1339-1353, 2012.

Tanre, D., Geleyn, J.-F., and Slingo, J. M.: First results of the introduction of an advanced aerosol-radiation interaction in the ECMWF low resolution global model, in: Aerosols and Their Climatic Effects, edited by: Gerber, H. and Deepak, A., Deepak Publishing, Hampton, VA, 133-177, 1984.

Taylor, K. E.: Summarizing multiple aspects of model performance in a single diagram, Journal of Geophysical Research, 106, 7183-7192, doi: 10.1029/2000JD900719, 2001.

Ummenhofer, C. C., D'Arrigo, R. D., Anchukaitis, K. J., Buckley, B. M., and Cook, E. R.: Links between Indo-Pacific climate variability and drought in the Monsoon Asia Drought Atlas, Climate Dynamics, 39, 16 pp., doi: 10.1007/s00382-012-1458-1, 2012.

Wang, B., Wu, R., and Lau, K. M.: Interannual variability of the Asian summer monsoon: contrasts between the Indian and the Western North Pacific-East Asian Monsoon, Journal of Climate, 14, 4073-4090, 2001.

Wang, B.: The Asian Monsoon, Springer/Praxis Publishing Co, Berlin, 2006.

Webb, R. W., Rosenzweig, C. E., and Levine, E. R.: Global Soil Texture and Derived Water-Holding Capacities, data set, available online under http://www.daac.ornl.gov (last access: 5. February 2013), Oak Ridge National Laboratory Distributed Active Archive Center, Oak Ridge, Tennessee, USA, 2000.

Weber, T., and Quaas, J.: Incorporating the subgrid-scale variability of clouds in the autoconversion parameterization using a PDF-scheme, Journal of Advances in Modelling Earth Systems, 4, M11003, doi: 10.1029/2012MS000156, 2012.

Webster, P. J., Magana, V. O., Palmer, T. N., Shukla, J., Tomas, R. T., Yanai, M., and Yasunari, T.: Monsoons: processes, predictability and the prospects of prediction, Journal of Geophysical Research, 103 (C7), 14451-14510, 1998.

Wells, N., Goddard, S., and Hayes, M. J.: A Self-Calibrating Palmer Drought Severity Index, Journal of Climate, 17, 2335-2351, 2004.

Wetzel, P., Maier-Reimer, E., Botzet, M., Jungclaus, J. H., Keenlyside, N., and Latif, M.: Effects of ocean biology on the penetrative radiation in a coupled climate model, Journal of Climate 19, 3973–3987, 2006.

Yatagai, A., Kamiguchi, O., Arakawa, A., Hamada, N., Yasutomi, N., and Kitoh, A.: APHRODITE: Constructing a Long-term Daily Gridded Precipitation Dataset for Asia based on a Dense Network of Rain Gauges, Bulletin of American Meteorological Society, 93, 1401-1415, http://dx.doi.org/10.1175/BAMS-D-11-00122.1., 2012.

Zanchettin, D., Rubino, A., and Jungclaus, J. H.: Intermittent multidecadal-to-centennial fluctuations dominate global temperature evolution over the last millennium, Geophysical Research Letters, 37, L14702, 6 pp, doi:10.1029/2010GL043717, 2010.

Tables

Tab. 1. Paleoclimatic records from India used in this study. Records are listed from North to South.

No	Name	ϕ (°N)	λ (°E)	Archive	Proxy	Reference
1	Sitikher bog, Spiti	32.30	77.43	Peat Bog	Pollen	Chauhan et al. (2000)
2	Gangotri	31.00	79.00	Sediment	Pollen	Kar et al. (2002)
3	Nepal	28.00	84.00	Stalagmite	Laminae thickness	Denniston et al. (2000)
4	Paradise Lake	27.30	92.06	Lake core	Pollen	Bhattacharya et al. (2007)
5	Narmada basin	23.00	77.43	Sediment	Flood deposit	Ely et al. (1999)
6	Lonar	19.51	76.00	Lake sediment	Geochemistry	Prasad et al. (2013)
7	Dandak	19.00	82.00	Stalagmite	$\delta^{18}O$ Isotope	Sinha et al. (2011a)
8	Jhumar	18.52	81.52	Stalagmite	$\delta^{18}O$ Isotope	Sinha et al. (2011a)
9	Godavari	16.00	83.00	Marine Core	Biomarker isotopes	Ponton et al. (2012)

Tab. 2. Temporal correlation coefficients and the statistical significance at the 99% confidence level between AIMR (JJAS), TSI (JJAS), ONI (annual) and DMI (annual) averaged over the 200-yr climatology of MWP, LIA and REC.

	MWP				***LIA***				***REC***			
	AIMR	**TSI**	**ONI**	**DMI**	**AIMR**	**TSI**	**ONI**	**DMI**	**AIMR**	**TSI**	**ONI**	**DMI**
AIMR	1.0	-0.95 (99%)	-0.63 (99%)	-0.59 (99%)	1.0	-0.94 (99%)	-0.61 (99%)	-0.47 (99%)	1.0	-0.94 (99%)	-0.66 (99%)	-0.56 (99%)
TSI	-0.95 (99%)	1.0	0.67 (99%)	0.65 (99%)	-0.94 (99%)	1.0	0.66 (99%)	0.55 (99%)	-0.94 (99%)	1.0	0.74 (99%)	0.64 (99%)
ONI	-0.63 (99%)	0.67 (99%)	1.0	0.64 (99%)	-0.61 (99%)	0.66 (99%)	1.0	0.59 (99%)	-0.66 (99%)	0.74 (99%)	1.0	0.69 (99%)
DMI	-0.59 (99%)	0.65 (99%)	0.64 (99%)	1.0	-0.47 (99%)	0.55 (99%)	0.59 (99%)	1.0	-0.56 (99%)	0.64 (99%)	0.69 (99%)	1.0

Figures

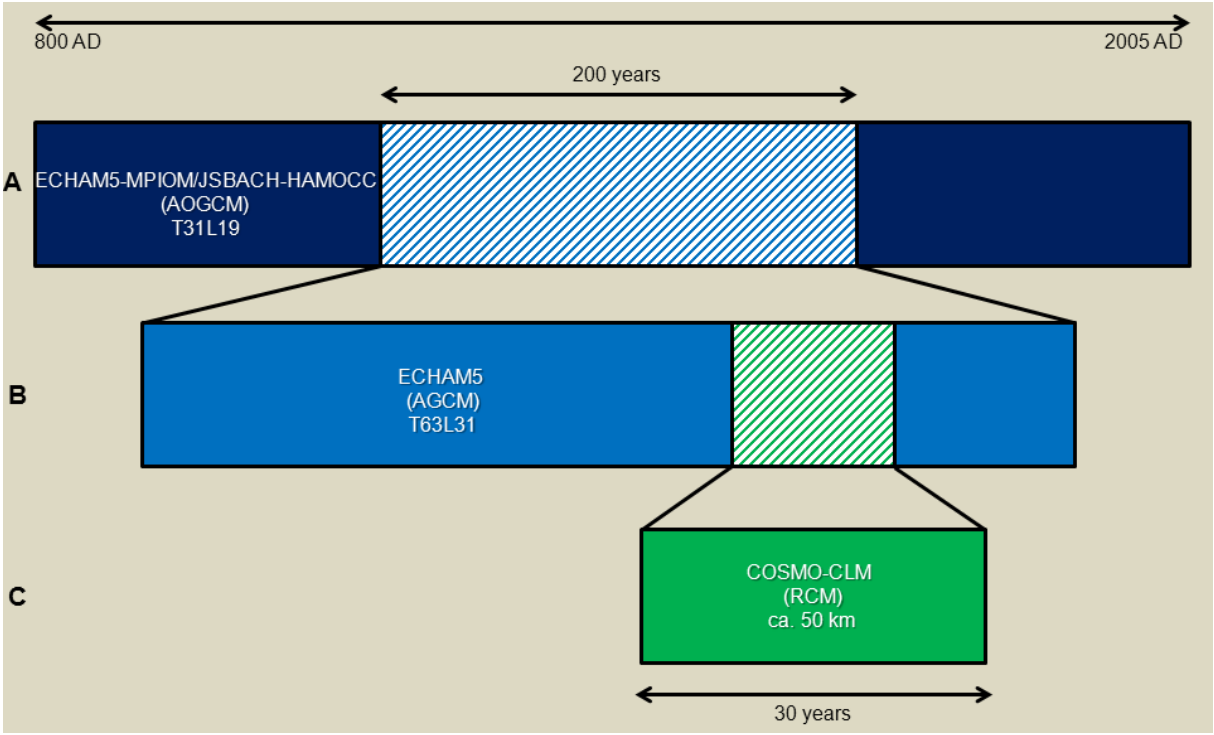

Fig. 1. Conceptual simplified framework of global (dark and light blue) and regional (green) climate simulations in HIMPAC and CADY project for the last Millennium 800-2005 AD. A – Millennium Experiment using fully coupled AOGCM in T31L19 spatial resolution (ECHAM5). B – Atmosphere-only 200 years - time slices experiments using ECHAM5 Model in T63L31 horizontal resolution. C – High resolution regional climate model simulations with COSMO-CLM in a 50 km spatial resolution for 30 years - time slices.

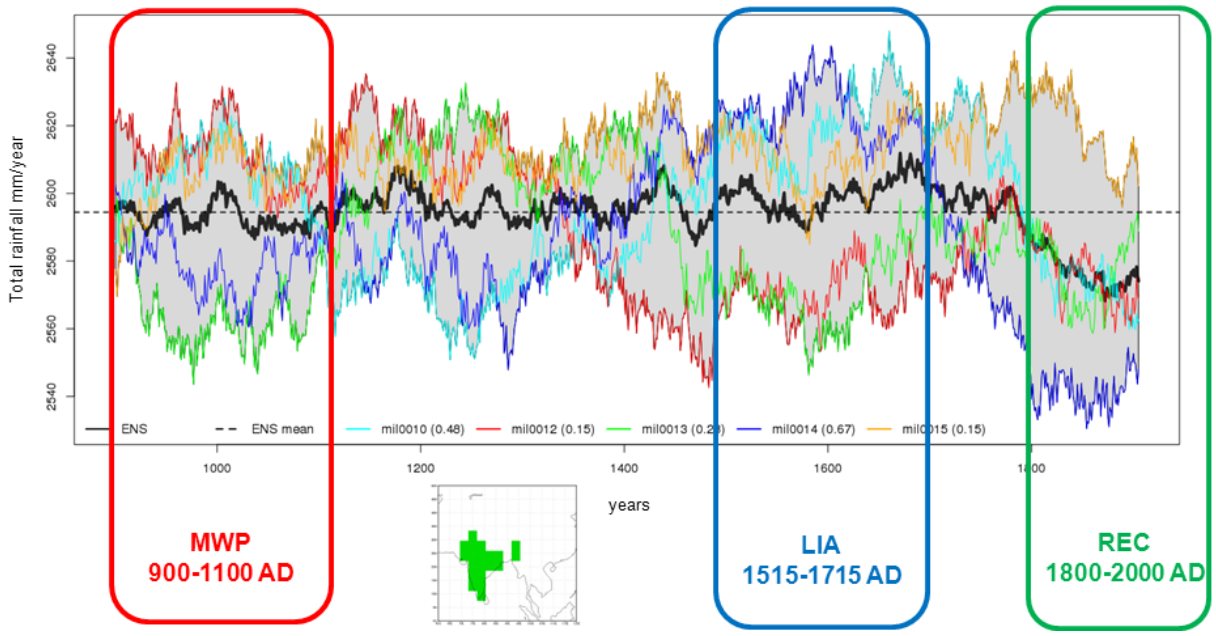

Fig. 2. Annual total rainfall in mm/year as 200 years running mean for five ensemble members mil0010 – mil0015 of Millennium Experiment using ECHAM5/MPIOM-JSBACH/HAMOCC in T31L19 horizontal resolution (ECHAM5); 800-2005 AD averaged over AIMR (All India Monsoon Rainfall) grid boxes (small figure). The ensemble mean is shown as black solid line. The climatological mean of all ensemble members is represented by the dashed black line. The selection of time slices for the ECHAM5 simulations in T63L31 are shown by the boxes for the Medieval Warm Period (MWP; 900-1100 AD) in red, the Little Ice Age (LIA; 1515-1715 AD) in blue and the Recent Climate Period (REC; 1800-2000 AD) in green. The selection has been done according to the highest temporal correlation of ensemble member mil0014 (temporal correlation = 0.67; dark blue solid line) to the ensemble mean and the characteristic warm and cold temperature signals during MWP and LIA.

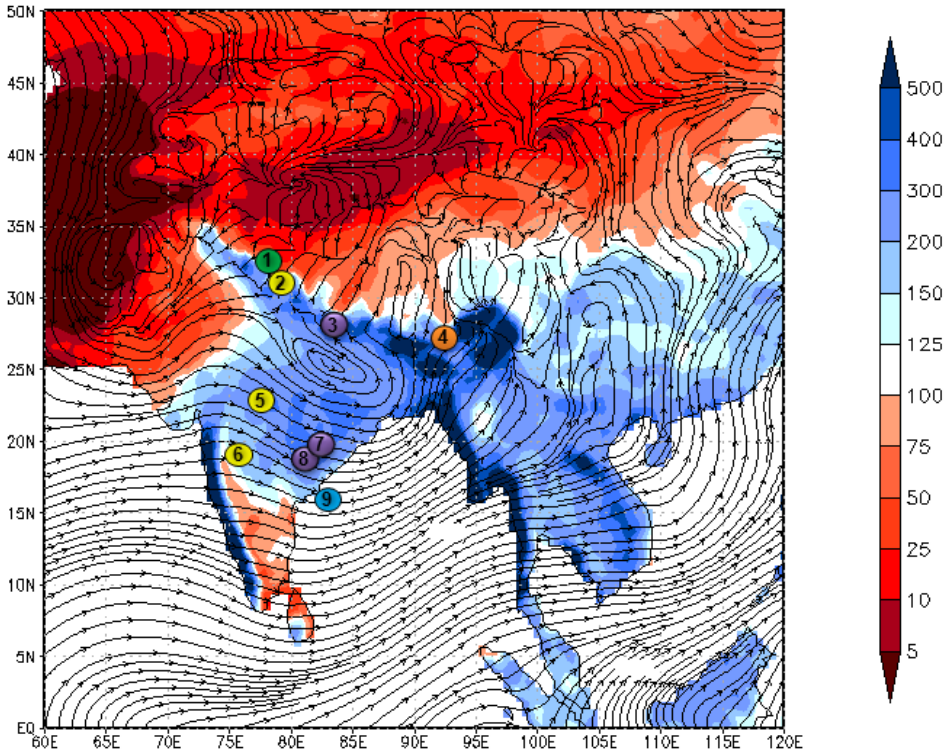

Fig. 3. Study area with climatological land surface summer monsoon rainfall (JJAS) for GPCC5 data set from 1901-2009 (mm; shaded colours), summer monsoon (JJAS) lower tropospheric wind fields (streamlines) at 850 hPa for ERA-Interim reanalysis data set from 1989-2011 and the spatial coverage of the Indian paleoclimatic records considered in this study as numbered dots. Numbers of the nodes were assigned according to the geographical coordinates of the respective study site and furthermore refer to the entries in Tab. 1. Sites that are at close proximity might show displaced to prevent overlap of the dots and labels. Colours of the dots indicate the type of archive: green – peat bog, yellow – sediment sites, orange – lake core, purple – stalagmites and blue – marine core.

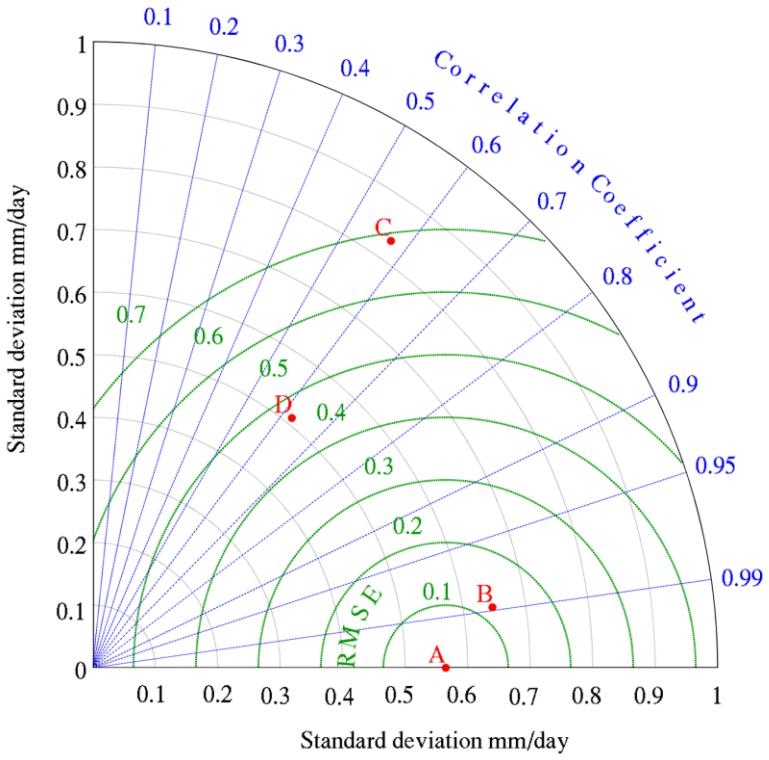

Fig. 4. Taylor diagram for rainfall time series analysis between observation data: APHRODITE (A) and GPCC6 (B) and climate model simulations: ECHAM5 Model in T63L31 spatial resolution (C) and MPI-ESM realization mil0014 with ECHAM5 Model in T31L19 spatial resolution (D) for summer monsoon (JJAS) 1951-2000. The statistical parameters are based on the APRHODITE (A) reference data set averaged over 0-50°N and 60°-120°E.

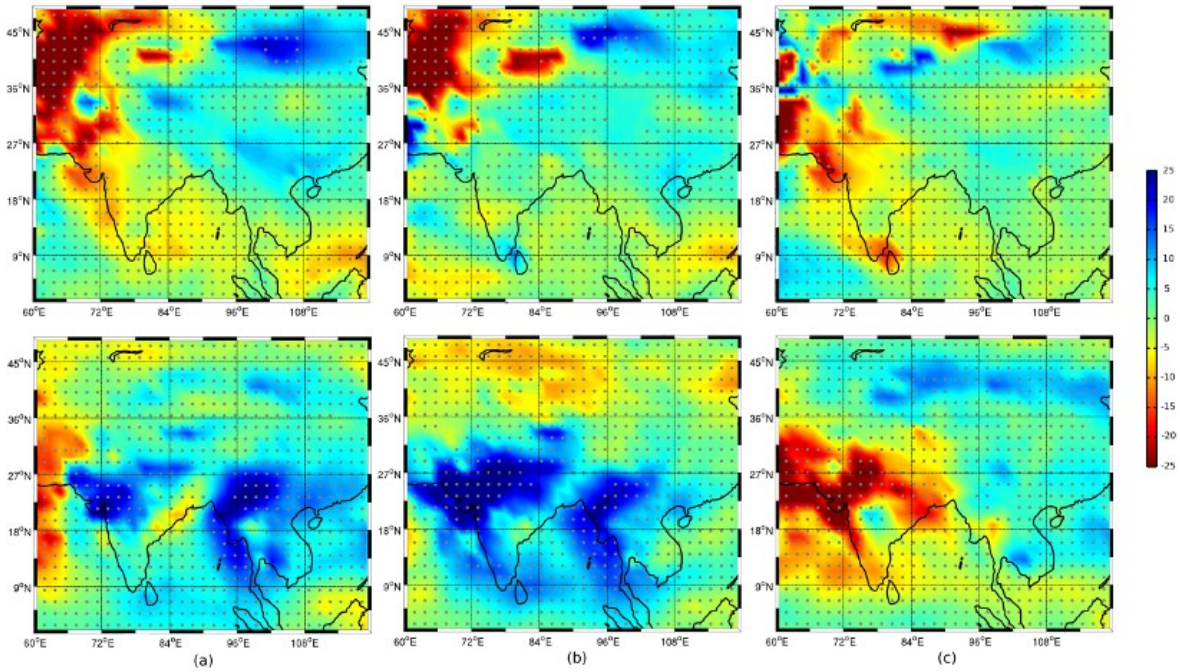

Fig. 5. Anomalies of precipitation (%; colours) and its statistical significance at 95% confidence level (gray dots) for ECHAM5 in summer monsoon (JJAS; upper panel) and winter monsoon (DJF; lower panel) “MWP minus REC” (a), “LIA minus REC” (b) and “MWP minus LIA” (c).

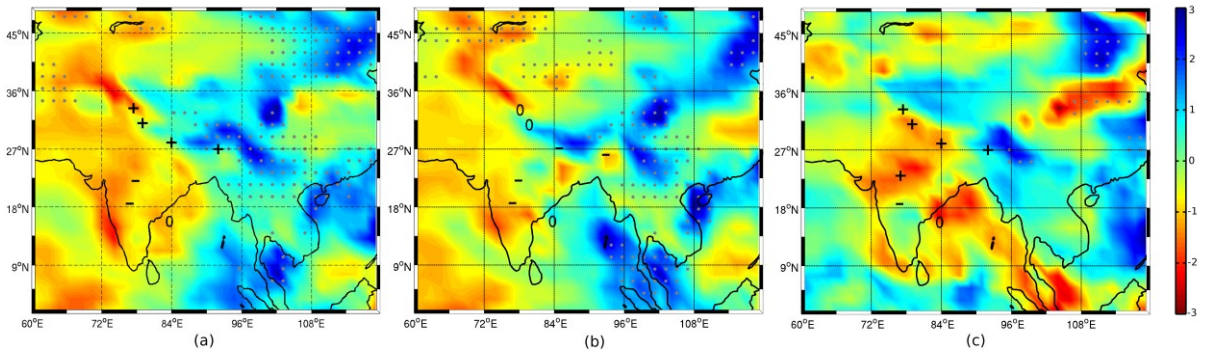

Fig. 6. Normalized annual P-E anomalies (mm; colours) and its statistical significance at 95% confidence level (gray dots) for ECHAM5 Model and reconstructed moisture index (symbols: "+" wetter, "-" drier and "0" no changes); dimensionless;) for "MWP minus REC" (a), "LIA minus REC" (b) and "MWP minus LIA" (c).

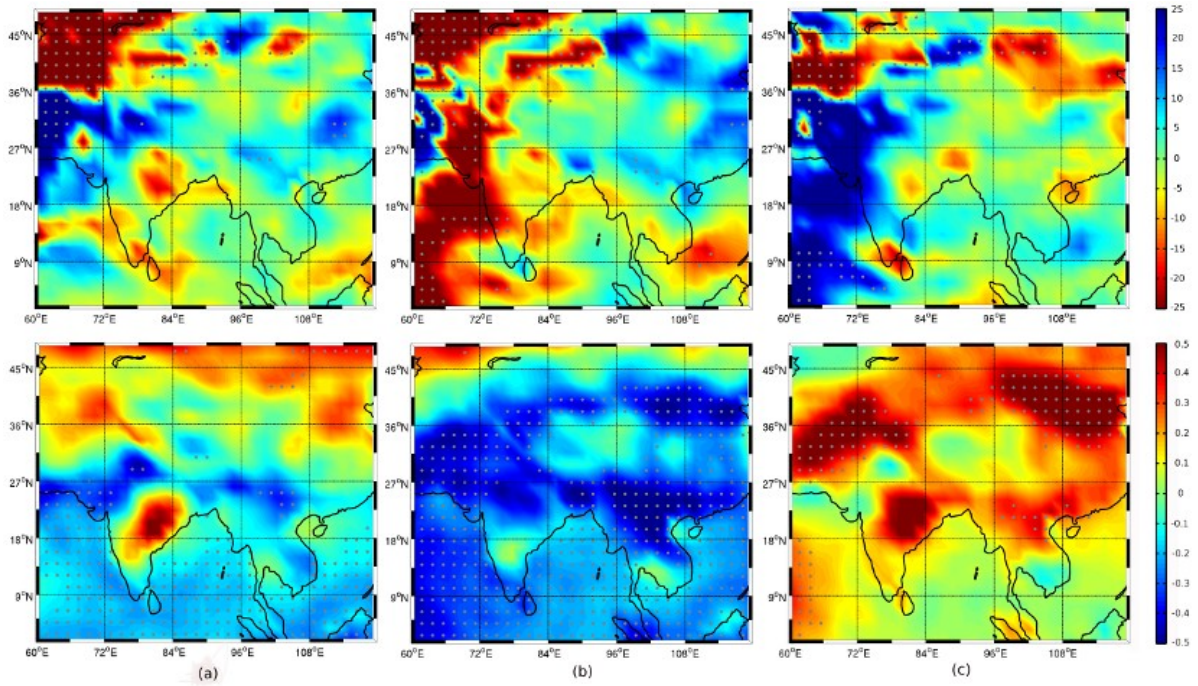

Fig. 7. Anomalies of precipitation “dry monsoons” (%; colours) for ECHAM5 shown in upper panel. Differences in 2m-air temperature “dry monsoons” (K; colours) for ECHAM5 shown in lower panel for “MWP minus REC” (a), “LIA minus REC” (b) and “MWP minus LIA” (c); summer monsoon (JJAS). Additionally the statistical significance at 95% confidence level is marked as gray dots.

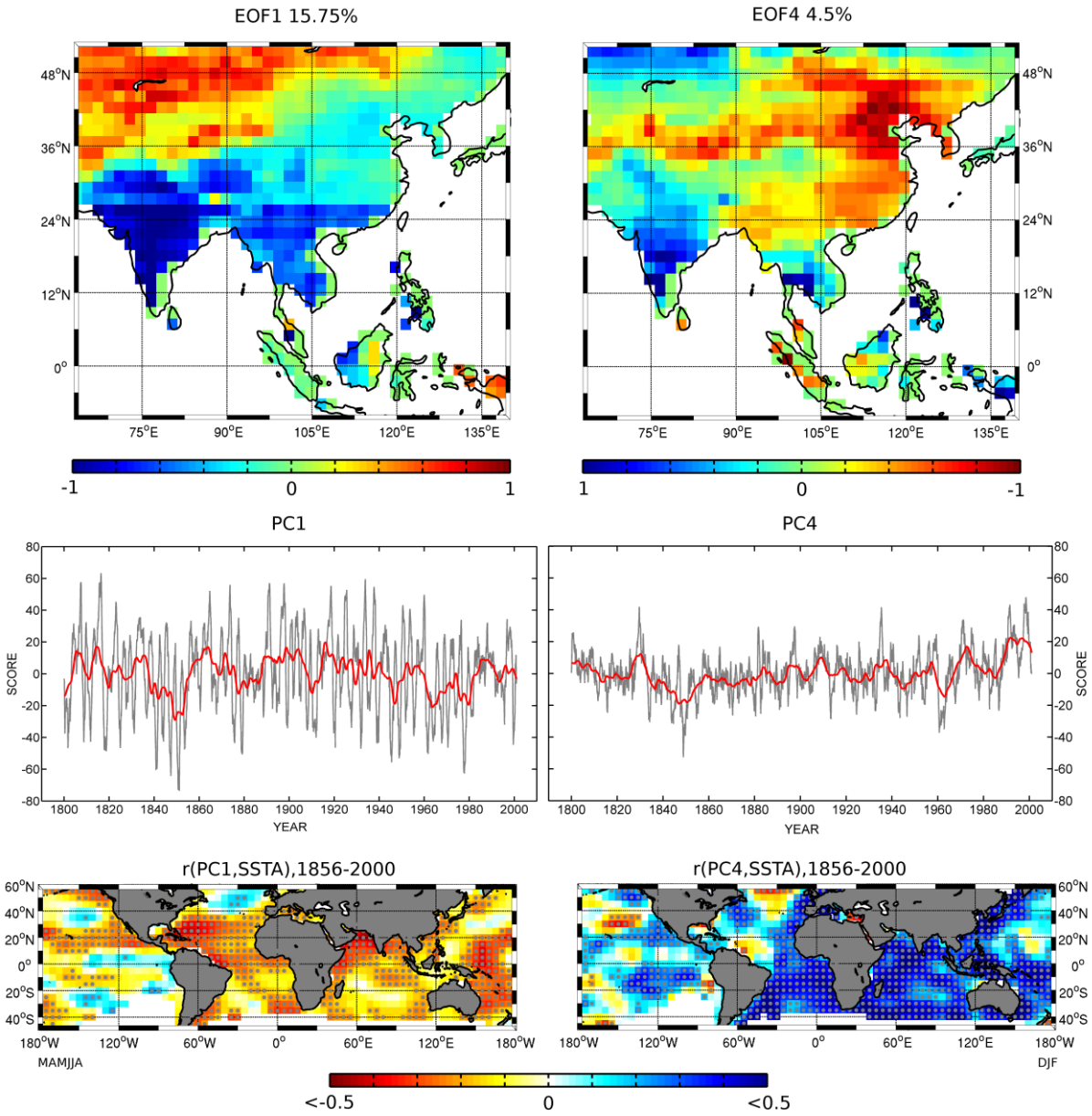

Fig. 8. Spatiotemporal patterns of the PDSI from 1800-2000 AD. Empirical orthogonal function (EOF) analysis of the PDSI with two distinct modes (EOF1 and EOF4) is shown here. The middle panels illustrate the time series expansion (PCs, principal components) of the corresponding spatial modes in the top row. In the lower row, Pearson correlations with Sea Surface Temperature Anomalies (SSTA) and EOF/PC1 are simultaneous with the monsoon and pre-monsoon season (MAMJJA), whereas the SSTA patterns for EOF/PC4 are for the previous winter (DJF) season. The significant correlation values at 95% confidence level are marked by gray dots.